JOURNAL OF GEOPHYSICAL RESEARCH, VOL. 106, NO. A5, PAGES 8301–8313, MAY 1, 2001

Whistler waves, Langmuir waves and single loss cone electron distributions inside a magnetic cloud: Observations

O. Moullard,[1] D. Burgess,[2] C. Salem,[3] A. Mangeney,[3] D. E. Larson,[4] and S. D. Bale[4]

Abstract. Whistler waves propagating along the ambient magnetic field are observed within a coronal mass ejection (on January 10, 1997) associated in time with Langmuir waves and electron distributions of a single loss cone type. In addition, background observations are made on the plasma wave activity in the sheath and foreshock regions that precede the magnetic cloud, on the observed radio emissions (including a type II radio burst) and on the geometry of the cloud. All the data comes from the WIND spacecraft. The whistler waves are identified using full magnetic waveforms while possible evidence of coexisting parallel, and antiparallel propagating Langmuir modes are found in the waveform and spectral wave data from the WAVES experiment. A few hundred low energy electron distributions from the Three-Dimensional Plasma (3DP) experiment are investigated. Finally, we tentatively suggest that this type of plasma wave particle activity is linked to the type II emission observed, i.e., that the emission mechanisms are proceeding and taking place within the magnetic cloud instead of at the shock region as usually thought. The extra suprathermal electrons could source from electrons accelerated at reconnection sites between the magnetic cloud and the ambient interplanetary magnetic field. A linear instability study using observed properties of the electron distributions is to be presented in a following paper.

1. Introduction

Plasma wave activity has not been much investigated inside magnetic clouds. Low frequency electromagnetic (EM) waves have been observed in the solar wind in association with Langmuir waves, sometimes together with ion acoustic waves [*Kennel et al.*, 1980; *Thejappa et al.*, 1995b; *Thejappa and Macdowall*, 1998]. These EM waves are usually primarly identified as whistlers from their frequency, below the electron cyclotron frequency f_{c_e}, and magnetic character (lower frequency branch of the electron cyclotron). Yet complete identification or further characterization (e.g., sense of polarization or comparing field and frequency dependent refractive indices) requires to infer the propagation angle from three orthogonal components [*Lengyelfrey et al.*, 1994]. Nonlinear wave coupling between a whistler wave and a Langmuir wave has been in general rejected in favor of these waves sharing only a common source of instability [e.g., *Kellogg et al.*, 1992]. For example, *Kennel et al.* [1980] consider dissimilar wave fluctuations as an evidence against wave coupling occuring. It is often said that oblique whistler wave vectors are required for the coupling; yet *Chian and Abalde* [1999] recently showed analytically that the coupling of parallel propagating whistler and Langmuir waves can result in a transverse wave. Observed on their own whistler waves are usually attributed to an electron heat flux instability, and distributions of a loss cone type or beams with a perpendicular temperature above the parallel are said to be unstable to whistlers.

Electron distributions in the (ecliptic) solar wind come in various shapes generally split into a "core" at low energy and a "halo" at higher energy, distinguished by a change of slope in the distribution typically within 50–100 eV [*Pilipp et al.*, 1987]. Often $T_{c_\parallel}/T_{c_\perp} \sim 1$, but $T_{h_\parallel}/T_{h_\perp} > 1.1$ (c, core; h, halo; $\perp$, perpendicular to $\mathbf{B}$; $\parallel$, parallel to $\mathbf{B}$; T, temperature). *Phillips et al.* [1996] observed several periods with suprathermal single loss cone distribution in ULYSSES data, with a loss in the antiparallel direction attributed to a antisunward strahl being mirrored back in a weak magnetic bottle (loss cone (half) angle was around 60°). These periods seemed associated to the forward and reverse shock of some corotating interaction regions.

Coronal mass ejections (CME) which are fast enough to drive a shock are often observed associated with solar radio type II bursts. A type II signature is recognized on a radio spectrogram as a relatively narrow band emission that

[1]Space Science Department, European Space Agency, Noordwijk, Netherlands.
[2]Astronomy Unit, Queen Mary and Westfield, London, United Kingdom.
[3]Département de Recherche Spatiale, Observatoire de Paris-Meudon, Meudon, France.
[4]Space Sciences Laboratory, University of California, Berkeley, California.

Paper number 2000JA900144.
0148-0227/01/2000JA900144$09.00

drifts toward lower frequencies with time (see for numbers *Reiner et al.* [1998a]). With a density model this frequency drift converts to the shock front speed. Consequently type II emission is usually thought to be generated by shock accelerated electrons at the fundamental and/or the harmonic of the local plasma frequency [*Reiner et al.*, 1998b]. Recently, *Bale et al.* [1999] observed fast electrons and Langmuir waves upstream of an interplanetary shock time correlated with what they considered to be a type II burst observed in situ (emission seen briefly 1 day before and at the shock).

Here whistler waves propagating along the ambient magnetic field (identified with full B waveform data) and waves at near the plasma frequency (f_{p_e}) considered to be Langmuir waves (with possible evidence of coexisting parallel and antiparallel propagating modes) are observed very well time correlated with single loss cone electron distributions in two active periods within a magnetic cloud. This plasma wave particle activity could be linked to the type II emission observed, in which case the type II emission mechanism proceed and take place within the magnetic cloud instead of at the shock region as usually thought. The observation is made using WIND spacecraft data.

2. Magnetic Cloud Observed on January 10, 1997

The coronal mass ejection (CME) in this case study is the "ISTP event" from January 6 to 11, 1997 that has been tracked from Sun to Earth by conjugate observation from the International Solar Terrestrial Program (ISTP) spacecraft and ground stations [*Webb et al.*, 1998; *Fox et al.*, 1998; *Reiner et al.*, 1998a]. The front of the magnetic cloud associated to this CME is detected by the WIND spacecraft ($\sim$ 100 R_e from Earth) instruments on January 10, 1997 at 0445 UT (Figure 1). From January 10 at 0815 UT to January 11 around 0100 UT, the magnetic field rotates very smoothly as indicated by its latitude θ decreasing almost linearly with time from 175° to 25°, its longitude ϕ constant at 230° (in GSE coordinates), a near constant and relatively large amplitude $B = 14$ nT. The proton plasma beta is very low $\beta \sim 0.02$. This is a classical magnetic cloud signature consistent with a two-dimensional magnetic rope structure [review by *Burlaga*, 1991]. The magnetic field is strongly southward then strongly northward after rotation, with its B_z component varying from -10 nT to 10 nT, i.e., rotating by $\theta \sim 180°$. The global magnetic field geometry is of "south-west-north" type [*Mulligan et al.*, 1998], with an axial magnetic field in the ecliptic plane and a positive helicity, i.e., a right-hand twist along the axial field.

The whole observed interplanetary CME structure (see caption in Figure 1) can be seen as a region of increased and rather obviously related fluctuations of B and n (and V_{SW}) from January 10, 1997 at 2000 UT to January 11, 1997 at 0800 UT, marked by a transition from a slow wind ($V_{SW} = 375$ km s^{-1}) to a fast wind ($V_{SW} = 550$ km s^{-1}). The end of the magnetic cloud in the strict sense is marked by the presence of a compressed trailing density region [*Burlaga et al.*, 1998] starting from January 10, 1997 at around 2000 UT. Inside the high density region (peak at $n = 43$ cm^{-3}), the magnetic field is also compressed and peaks at 25 nT. However, the magnetic field also drops dramatically down to $B = 0.7$ nT on January 11, 1997 at 0345 UT. This large dip in the magnetic field or magnetic hole lasts about half an hour at $V_{SW} = 450$ km s^{-1}, thus it is almost a million kilometers long. This magnetic hole has a very high $\beta \sim 100$ and is approximately associated with a negative density gradient together with a positive velocity gradient, so that the magnetic hole could be related to a thin current sheet. In fact there is a second magnetic hole on January 11, 1997 at 0545 UT. The rear of the magnetic structure of the CME is consistent with a magnetic doughnut shape. Besides the twisting of the magnetic field lines around the axial field, one can imagine that before eruption the anchored loop structure

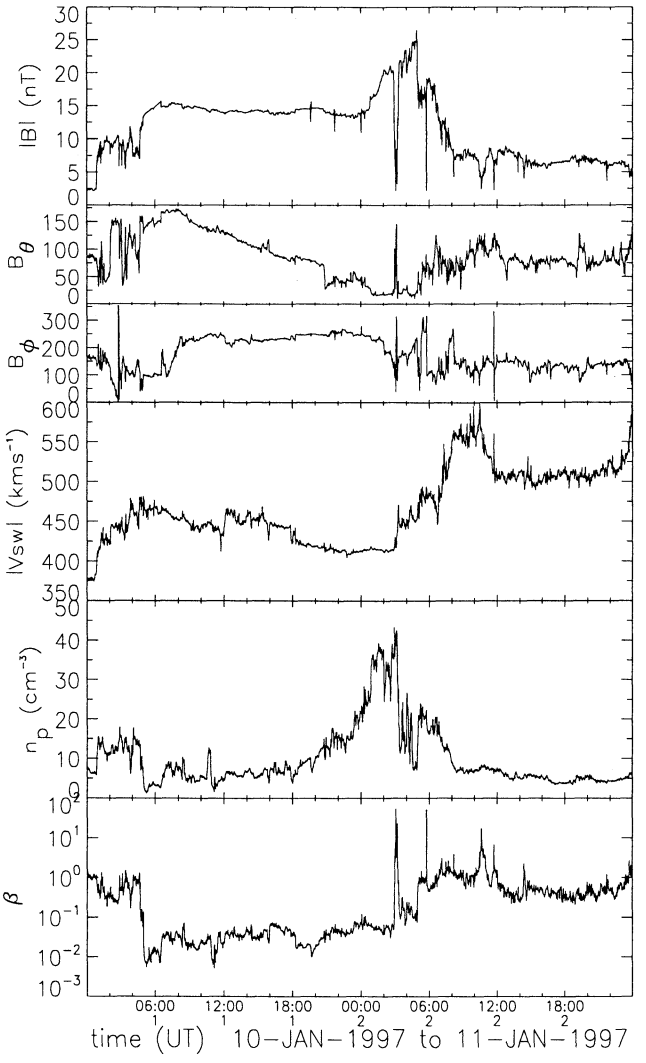

Figure 1. CME event on January 10 and 11, 1997: in chronological order, the observed interplanetary CME is structured into a sheath (following a shock), a magnetic cloud, a trailing high density region with two magnetic holes, a trailing sheath and is followed by a fast solar wind stream. (top to bottom) $|\mathbf{B}|$, B_θ, B_ϕ, $|\mathbf{V}_{SW}|$, n_p and β.

twisted by 180° around its expanding direction (radial) and subsequently reconnected where the knot was formed. The escaping closed structure would logically have a doughnut shape with a magnetic depression inside. Such a twisting is also compatible with the eccliptic plane magnetic field in the hole being found opposite to the one inside the cloud in a region where B_z approaches zero. To complete these general observation, one notices that the magnetic field direction is radial before and after the CME event.

3. Interplanetary Shock and Type II

The CME drove a shock in the interplanetary medium and was associated with solar type II radio emission. At 1 AU, on January 10, 1997 at 01:00 UT, the shock is characterised by a jump discontinuity increasing the magnetic field amplitude by a factor 4 and the density by a factor 2, as well as an average ejecta speed (465 km s^{-1}) greater than the ambient solar wind speed (380 km s^{-1}). In absolute numbers, the proton density n jumped from 6.8 cm^{-3} to 13.2 cm^{-3}, B from 2.3 nT to 9.0 nT, and β from 1 to 0.5 (with large fluctuations in the sheath). This density measurement comes from the Solar Wind Experiment (SWE) and the magnetic field data from the Magnetic Fields Investigation (MFI). The type II emission initially appears on the WAVES-TNR spectrogram (Figure 2) at 250 kHz on January 8, 1997 and is intermittently seen until January 10, 1997. On this day it appears as multiple bands slowly drifting of frequency within 50–100 kHz (top panel of Figure 2). More than one type II signature is found which means there are many emission sites along the CME driven shock. *Reiner et al.* [1998a] located some of the emission sites on January 8, 1997 to be upstream of the shock when it interacted with a corotating interaction region (CIR), which characteristic solar wind speed pattern is seen in the days nearby the observed magnetic cloud. There is no obvious sign of local type II emission in the shock region on January 10, 1997.

There is no indication of any type II emission occurring (locally) in the sheath of the magnetic cloud. According to the type II signature on the spectrogram during this period, the emission would have to be at $2f_{p_e}$. There is a $2f_{p_e}$ emission line (with some bursts), but it appears to be emission from the terrestrial foreshock because its frequency variations are delayed relative to the plasma line at f_{p_e}. Additionally, the $2f_{p_e}$ emission line does not have a frequency closely matching any of the type II drifting bands.

The low-frequency (below f_{p_e}) emission is typical of a class of interplanetary shock, with enhanced electrostatic (ES) activity upstream and enhanced EM emission downstream [*Thejappa et al.*, 1995a]. The upstream ES waves ap-

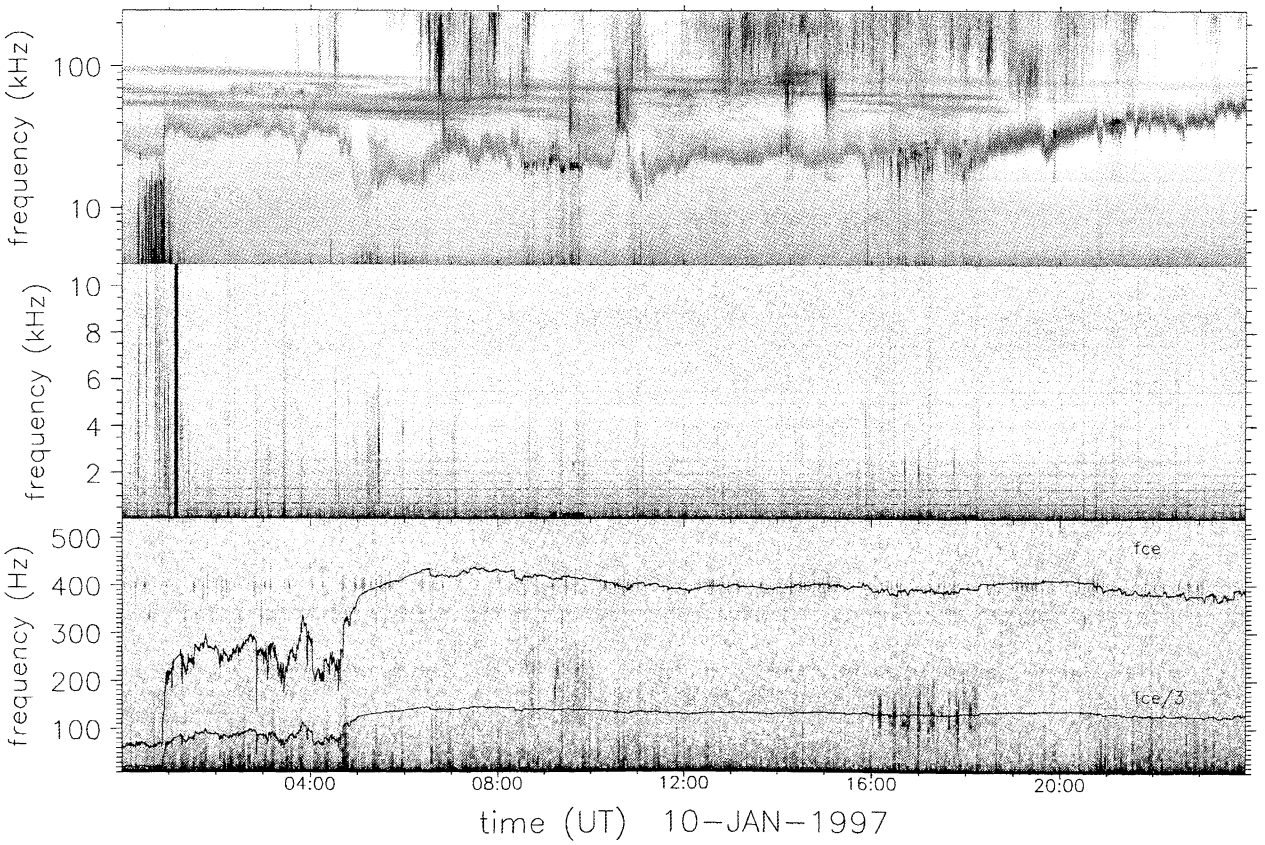

Figure 2. Some electric and magnetic spectrograms from WIND-WAVES during the interplanetary CME on January 10, 1997. See description in Sections 3 and 4. (top to bottom) TNR spectrum (electric, 4–256 kHz), FFTH spectrum (electric, 21.3 Hz–10.4 kHz), portion of FFTM spectrum (magnetic, 5.3–540 Hz). The whistler active period (see series of bursts near the $f_{c_e}/3$ curve in the magnetic spectrum) are at 0830–1000 UT and 1600–1830 UT.

pear at first sight to be ion acoustic waves strongly doppler shifted in frequency up to around 10 kHz. A closer inspection of the FFTH spectrum shows that the ES wave activity before 01 UT is enhanced at different times in 3 frequency ranges (1–3 kHz, 3–6 kHz, 4–10 kHz) rather than being a series of broadband signals of frequency up to 10 kHz as seen on the spectrogram. Only some of these upstream ES waves can be ion acoustic waves doppler shifted by the solar wind since the maximum doppler shift is $V_{\rm SW}/(2\pi\lambda_D) \sim 7\ kHz$, with the observed values $V_{\rm SW} = 380$ km s^{-1}, debye length $\lambda_D = 9$ m^{-1} ($T_e = 7$ eV, $n = 5$ cm^{-3}), $\cos\theta_{kV} = 1$, and for a wave vector parallel to the interplanetary magnetic field. The downstream EM waves, of frequency below $f_{\rm c_e}/3$, are likely whistler waves.

Additionally, the radio type II emission and other radio emission are observed while the magnetic cloud hits the Earth's magnetosphere (reconnection occurs). First some auroral kilometric radiation (AKR) is seen in the WAVES-TNR spectrogram (Figure 2). AKR is intense and broadband radio emission from the Earth's magnetosphere, typically observed in the frequency range 100–500 kHz [*Kurth et al.*, 1998]. The AKR might well relate to the increase of relativistic electrons (above MeV) observed in the outer Earth's radiation belt [*Buhler et al.*, 1998]. Additionally some multiple narrowband emission drifting up in frequency is seen between 0900 UT and 1030 UT within the frequency range 80–200 kHz. The emission consists of two (or three) bands that appear harmonically related, are separated by roughly 80 kHz (or 40 kHz), and drift up by $\sim$ 100 kHz in an hour. This emission is faint relative to the intense AKR and radio type II. Could that emission be harmonics of an Earth's magnetospheric emission?

4. Plasma Wave Activity

The input for the WAVES instruments on board WIND (TDS, FFT, TNR, RAD1, RAD2) comes from three orthogonal electric dipolar antennas and a tri-axial magnetic search coil, although only the lower frequency detectors (TDS, FFT) benefit from a magnetic input. Effective antenna lengths are 43.5 m and 4.68 m for the spin plane wire antennas x and y, and 2.54 m for the rigid antenna along the spin direction (calculated by Bob Manning, Paris-Meudon Observatory). See *Bougeret et al.* [1995] for a pre-launch description of the WAVES experiment. In particular, the TDS (Time Domain Sampler) is a fast magnetic and electric waveform sampler functioning essentially in two modes: a mode called TDSF (TDS Fast) which captures events from the two spin electric (AC) input at a fast sampling rate, $f_s = 120$ kS s^{-1}, and another called TDSS (TDS Slow) which samples from four components of the electric (DC) and magnetic input at $f_s = 7.5$ kS s^{-1}. The waveforms are 2048 samples long, thus a TDSS event lasts about 0.27 s and a TDSF event lasts 17 ms. The WAVES data presented here was accessed using the version 1.7d of the Windlib database package (see acknowledgments).

A general view of the plasma wave activity on January 10, 1997 can be seen in Figure 2, which displays some electric and magnetic spectrograms from the spectrum analyzer TNR (Thermal Noise Receiver) and the swept-frequency detector FFT (Fast Fourier Transformer). The input is from the x sensors. The full frequency range of TNR (4–256 kHz) and of the FFTH (FFT High) band (21.3 Hz–10.4 kHz) are represented for the electric spectrum and a portion of the FFTM (FFT Medium) band (otherwise ranging 5.3 Hz–2.7 kHz) for the magnetic spectrum. The FFT sweeps three frequency bands.

Noticeable features in the spectrograms are: (1) for TNR the multi-band radio type II, the trailing density region (increase of $f_{\rm p_e}$) and Langmuir waves (enhanced plasma line at $f_{\rm p_e}$), (2) for FFTH the ion acoustic broadband and narrowband spikes (also in TNR) and a low-frequency "ion acoustic continuum", (3) for FFTM a low-frequency "whistler continuum" and two distinct periods of whistler wave activity, 0830–1000 UT and 1600–1830 UT, appearing as series of bursts near the $f_{\rm c_e}/3$ curve. These waves will be shown to be whistlers. The expressions "active period" and "quiet period" will herein define periods with and without these waves, respectively. The plasma activity within the two (whistler) active periods is the main focus of this study.

Two distinctive periods of whistler activity are found within the magnetic cloud, the first one at 0830–1000 UT observed within the frequency range 120–280 Hz peaking at 220 Hz ($0.53 f_{\rm c_e}$), the second at 1600–1830 UT of frequency range 70–210 Hz and peak frequency at 115 Hz ($0.3 f_{\rm c_e}$). Appropriate waveform data from the TDS waveform sampler is available for the second period only. Minimum variance analysis of the magnetic field waveforms leads to a strong identification of the waves as whistlers (see next paragraph for detail and results). The two relevant real solutions (small negative or positive doppler shift) of the observed whistler wave dispersion relation are found to have an observed polarization consistent with being whistlers, based on their wave speed relative to the solar wind speed. The case of negatively doppler shifted wave frequency, corresponding to an antiparallel propagating wave, will be detailed in numbers.

These two whistler active periods are associated in time with electric oscillations at frequency near $f_{\rm p_e}$ considered here as Langmuir waves. In the TNR spectrogram, the Langmuir waves appear as an enhancement of the plasma line, i.e., the "line" of thermal emission near $f_{\rm p_e}$. Electric signals at near $f_{\rm p_e}$ that have large intensity are usually considered to be ES rather than the electric part of an EM signal. Also, similar observed waves have been found likely to propagate parallel to the background magnetic field [*Kellogg et al.*, 1999], in favor of the view that these are Langmuir waves. During the two whistler active periods, the emission at near the plasma frequency (20–25 kHz) appears complex with side bands on either side of $f_{\rm p_e}$ and short time scale structure in the waveforms. Maximum electric field amplitudes in the plasma line (delimited using the spectro-object method described by *Moullard* [2000]) are 14 μV m^{-1} (0.73 μV m^{-1} Hz$^{-\frac{1}{2}}$ when normalised by the frequency integration band) for the first whistler active period and 6.2 μV m^{-1} (0.38 μV m^{-1} Hz$^{-\frac{1}{2}}$) for

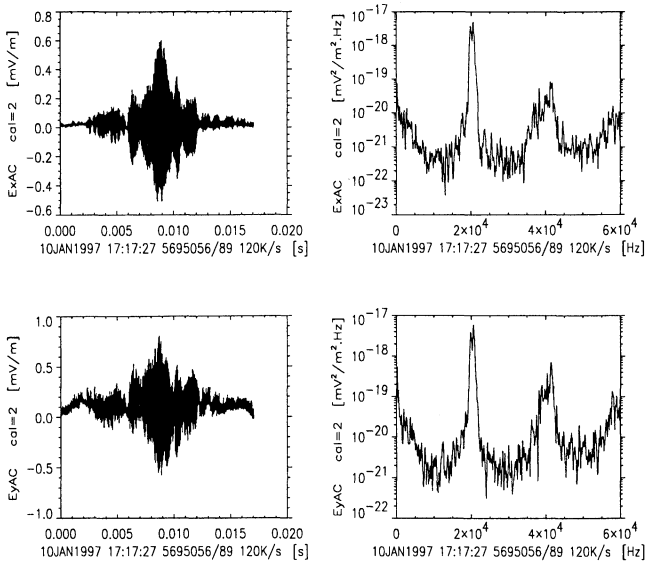

Figure 3. A TDSF Langmuir waveform found during the second whistler active period on January 10, 1997. Note the $2f_{p_e}$ feature ($\sim$ 40 kHz).

the second period. The fast sampled electric TDSF waveforms captured during the whistler active periods are essentially f_{p_e} emission (Figure 3). Their power spectra show broad peaks around f_{p_e}, sometimes resolved into double or multiple peaks, and cases of weaker $2f_{p_e}$ peaks. Most of these Langmuir waveforms have a rather transient aspect. The peak frequency of the f_{p_e} emission varies between 20–25 kHz. Langmuir waveforms are observed with electric field amplitude E_L mostly within $\sim$ 0.5–1.5 mV m^{-1} else $\sim$ 0.01 mV m^{-1} in some weaker events. The transient aspect of these Langmuir waveforms could well be a combination of an ion acoustic solitary event [see *Mangeney et al.*, 1999] and oscillation at f_{p_e}. Nevertheless, such waveforms have been described as "foreshock Langmuir solitons" [*Kellogg et al.*, 1999]. The multiple peaks indicate simultaneous emission at frequency $0.8f_{p_e}$ (lower limit) and near and above f_{p_e}. These complex power spectra correspond with what is seen in the TNR spectrogram on a smaller timescale: bursts near f_{p_e} together with side bands on either side of f_{p_e}. This suggests parametric decay may occur. Emission at $2f_{p_e}$ is seen on the power spectrum of many of the Langmuir waveforms, as in the figure example.

There may be some (doppler shifted) ion acoustic waves associated in time with the active periods, as indicated by some sporadic electric spikes in the FFTH (with no magnetic signal in the FFTM magnetic spectrum), although this is not a strong enhancement compared with the rest of the magnetic cloud. The broadband electric spikes in TNR below but reaching up to f_{p_e} are more likely caused by aliasing owing to the strong f_{p_e} emission. At frequencies below f_{p_e} in the TDSF ion acoustic observational range, only one sinusoidal waveform is found during the whistler active periods and the other waveforms are (ion acoustic) solitary like. This near monochromatic waveform, captured at 0941 UT, has a frequency 2.5 kHz and an electric amplitude 0.1 mV m^{-1}. The narrow band emission is also seen in the FFTH spectrogram as short lived.

There is otherwise some background plasma wave activity to discuss. Some low-frequency ES wave continuum at frequency below 500 Hz, i.e., more or less the ion plasma frequency f_{p_i}, and some low-frequency EM wave continuum at frequency far below 100 Hz (consistent but not strictly identified as whistlers) are continuously present during the magnetic cloud. Most of the emission of frequency between 100–500 Hz is of electrostatic nature as indicated by the absence of magnetic signal in the FFTM spectrograms at frequency above 100 Hz outside of the whistler active periods. No particular doppler shifted (above f_{p_i}) ion acoustic wave activity is observed within the magnetic cloud compared to usual solar wind conditions [*Moullard*, 2000]. Sporadic broadband electric spikes are found consistently in both the TNR and FFTH spectrograms, and in the FFTH some narrow bandwith electric spikes (i.e., near monochromatic) are seen below 4 kHz. Some low-frequency bursts are observed within the magnetic cloud, in particular EM bursts of frequency below 100 Hz. However, none of these low-frequency emissions are enhanced during the two higher frequency whistlers periods. Noticeably, on January 10, 1997, the ratio f_{c_e}/f_{p_i} sometimes approaches one, which perhaps has some effect on the wave activity. For all the waves observed, agreement is found between the low duty cycle electric and magnetic analyzers data in different frequency range and the waveform data.The FFT spectrograms are marked by many horizontal lines, i.e., signals at some constant frequency, that are necessarily interference events. Such an interference line at 400 Hz in the FFTM magnetic spectrogram curiously happens to nearly coincide with the f_{c_e} line within the magnetic cloud, but it is not an electron cyclotron emission line.

5. Analysis of Whistler Waveforms

Regarding the whistler wave observations, a general remark can be made. The large magnetic fields found within magnetic clouds should favor the detection of whistler waves whose observed frequency range otherwise falls in the very low-frequency response range of the waves instruments.

A high concentration of slower sampled events (TDSS) is found in both (whistler) active periods. The TDSS mode is only favorable (including full magnetic waveform) during the second active period 1600–1830 UT. Among the 27 TDSS events found in this period, only one of them is mere "noise". The TDSS magnetic waveforms appear moderately monochromatic with an observed peak frequency within 100–145 Hz (average 119 Hz) matching the FFT observation. The observed frequency f' is here deduced from a fit to the detrended and despun waveform rather than from the power spectrum peak. The waveforms are quite modulated, and sometimes phase jumps are seen. The magnetic field amplitude $|B|$ varies within 0.08–0.35 nT (av-

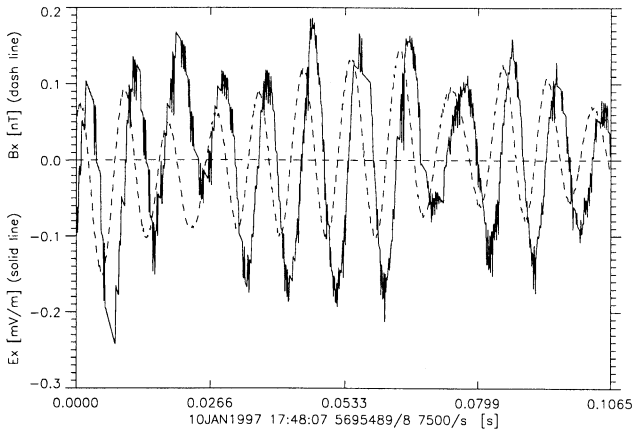

Figure 4. A whistler waveform on January 10, 1997. A 800 point-long sample of the electric field component E_x (solid line) and one magnetic field component B_x (dash line) after removal of the interference pattern and of the calibration trend. The wave electric field was exceptionally well-resolved by the WIND-WAVES-TDS sampler despite the DC interference pattern.

erage 0.2 nT). Remarkably, the wave electric field is often well-resolved by TDS in these events, despite the presence of a DC interference pattern. The electric fluctuations are seen in some portions of each TDSS sample as sinusoidal variations superimposed on the electric interference patterns. At poor resolution, the detrended electric waveform portion appears as a square like function varying between two values with a periodicity matching the magnetic field frequency. This indicates an electric amplitude of at most 0.1 mV m^{-1}, corresponding to half a telemetry number for these DC patterns. Other portions are better resolved (five telemetry numbers and more) in which case the sinusoidal aspect of the electric waveform is obvious. This is examplified in Figure 4 showing the exceptionally well-resolved electric fluctuations in TDSS event 9 at 174807 UT. The parallel refractive index $n_{||} = c|B|/|E| \sim c|B_x|/|E_x|$ is estimated from over three portions of length 100 points showing different modulations, $|E_x| = \{0.28, 0.25, 0.24\}$ mV m^{-1}, $|B_x| = \{0.17, 0.17, 0.16\}$ nT leading to $n_{||} = \{182, 203, 193\}$, i.e., $n_{||} = 190 \pm 10$, i.e., within $\pm 5\%$.

The same method of analysis as by *Moullard et al.* [1998] is applied to the waveforms: (1) the trend from calibration or spacecraft interference is fitted with a combination of low-frequency sinusoidal and second-order polynomial and removed, (2) waveforms are despun and transformed into GSE coordinates, and (3) minimum variance analysis is applied to the magnetic full field waveform. Only 10 waveforms are retained for which the low-frequency calibration trend was well removed (12 events out of 27) and with a good minimum variance quality (10 events out of 12). A good minimum variance quality is defined here by $(e_2/e_0, e_1/e_0) > (9, 9)$, i.e., the ratio of the eigenvalues in the maximum and intermediate variance directions $\mathbf{u}_2$ and $\mathbf{u}_1$ over the eigenvalue in the minimum variance direction $\mathbf{u}_0$ being above a threshold. A bad quality is usually found for waveforms with noisy portions, not well detrended or with large phase variations, so that this is not a bias against nonplanar waveforms.

A large minimum variance quality is found in the TDSS events varying from (11,14) up to (112,115) together with similar maximum and intermediate eigenvalues so that the waves are planar and quasi-circularly polarized. The waves propagate along $\hat{\mathbf{k}} = \pm\mathbf{u}_0$ with a direct angle between $\mathbf{u}_0$ and the IMF (equivalent to θ_{kB}) indicative of quasi-parallel propagation, i.e., $\theta_{kB} < 25°$ in all cases. The evolution of the wave magnetic field in the plane of field variations (u_1, u_2) shows that the waves are all right-hand polarized with respect to the IMF in the observation frame.

A cubic equation derived from the dispersion and doppler shift relations (in appendix A) is solved for deducing the wave number and the frequency f in the rest frame from the observed parameters. It is more correct than assuming $f = f'$ because the doppler shift can be quite important with θ_{kV} as small as 30°. With the parameters in this observation, two real solutions are found for the case of negative

Table 1. Characteristic Parameters for the Whistler Waveforms on January 10, 1997 1600–1830 UT.

f', Hz	θ_{kV}, deg	θ_{kB}, deg	f_{c_e}, Hz	f_{p_e}, kHz	k, km^{-1}	f, Hz	ω, rad s^{-1}	v_ϕ, km s^{-1}	$v_\phi \cos\theta_{kV}$, km s^{-1}	V_{SW}, km s^{-1}	n
128	26.8	21.8	381	26.7	-0.509	160	1010	-1970	-1760	448	152
117	45.3	9.5	391	22.3	-0.341	134	844	-2470	-1740	444	121
130	41.8	11.3	391	22.8	-0.384	150	945	-2460	-1830	443	122
101	34.4	18.0	390	22.7	-0.329	120	755	-2290	-1890	443	131
129	32.2	21.9	386	27.5	-0.516	159	1002	-1940	-1640	442	155
145	35.5	17.0	390	23.9	-0.461	172	1079	-2340	-1900	443	128
122	40.0	10.5	389	23.7	-0.384	143	898	-2340	-1790	445	128
108	27.1	24.2	386	25.9	-0.426	134	845	-1980	-1770	445	151
107	32.9	18.5	386	24.7	-0.384	130	817	-2130	-1790	444	141
117	34.3	18.6	393	22.1	-0.353	137	860	-2440	-2010	437	123

This is the negative doppler shift case, f_{p_e} is from 3DP ion density (very well behaved compared to SWE proton density during the active periods), n is the oblique refractive index (from rest frame frequencies), and f' is the observed frequency.

positive doppler shift and one real solution for the case of positive doppler shift. During both whistler active periods, $\mathbf{B_0} \cdot \mathbf{V_{SW}} > 0$ so that the positive doppler shift case corresponds to a wave propagating parallel to the magnetic field (negative and antiparallel, respectively). For this observation, both the parallel and antiparallel propagation solutions are consistent with a right-hand polarized wave in the rest frame (as required for low-frequency whistler waves) because $v_\phi \cos\theta_{kV}$ is always found greater than the solar wind speed. The parallel propagating wave solution and one of the two antiparallel propagating wave solutions have similar k and f (i.e., relatively small doppler shift), thus similar phase speed.

All relevant and deduced wave parameters for the case of negative doppler shift are reported in Table 1. The frequency of these waves in the rest frame f is $\sim$ 24 Hz on average above the observed frequency f', with f in the range 120–172 Hz, of mean $< f >= 144$ Hz. This leads to wave numbers k ranging -0.516–0.329 km^{-1}, of mean $< k >= -0.4$ km^{-1}, and oblique refractive indices n ranging 121–155, of mean $< n >= 135$, with $n \sim n_{\|}$. The phase velocity v_ϕ varies within -2470–1950 km s^{-1} and averages $< v_\phi >= -2240$ km s^{-1}. The parallel refractive index estimated from the field amplitudes for the ninth event of the table "9", $n_{\|} \sim 190$, compares well with $n_{\|} \sim 143$ calculated from the frequencies. This is an additional argument consistent with choosing a whistler dispersion relation. Estimates of the refractive index from the electric and magnetic field amplitude could in principle also be obtained from the FFT data, but this instrument has not yet been properly calibrated.

As an example for the positive doppler shift cases similar solution, consider the first waveform. The following characteristics are found: $k = 0.363\, km^{-1}$, $f = 105$ Hz, $f' - f = +23$ Hz, and $|v_\phi \cos\theta_{kV}| > |V_{SW}|$, i.e., $1620 > 448$ in km s^{-1} ($n = 166$). Larger refractive indices are found for lower rest frame frequency, i.e., for positive doppler shift than for negative doppler shift (true below $f_{c_e}/2$). For event 9, in the positive doppler shift case, $n_{\|} \sim 200$, which compares better with the field amplitudes refractive index. There is another case of negative doppler shift with, for the first waveform, $k = -3.4 km^{-1}$, $f = 344$ Hz, $f' - f = -216$ Hz, and $|v_\phi \cos\theta_{kV}| > |V_{SW}|$, i.e., $|-600| > 448$ in km s^{-1}. Note the very large doppler shift (large k) leading to a rest frame frequency near f_{c_e}. This third case with f near the resonance frequency f_{c_e} is not thought a viable solution; such a wave would be damped very quickly.

To summarize, for the second active period (with waveform data), the waves are EM, of frequency below f_{c_e}, planar, circularly polarized, and propagating along the background magnetic field. Together with the additional evidence (sense of polarization consistent in both observed and rest frame, observed electric field component leading to a reasonable match between field and frequency based dispersion indices), this unambiguously identifies the low-frequency waves as whistler waves.

6. Electron Distributions Observed

The electron distributions observed during the whistler (and Langmuir wave) active periods are very distinctive. They consist of largely increased suprathermal populations of single loss cone aspect relative to an average distribution found during a whistler quiet period.

By examining a daily contour plot of the electron distribution in pitch angle in the 250 eV energy band [*Larson et al.*, 2000], the whistler wave activity was found associated in time with a much increased electron population in the parallel direction for the 0830–1000 UT period and in the antiparallel direction for the 1600–1820 UT period. Electrons of energy 250 eV are halo electrons of speed $\sim$ 9400 km s^{-1}. In the rest of the magnetic cloud, there is either no apparent asymmetry in the electron distribution in pitch angle at 250 eV or a weaker unidirectional streaming or a bidirectional streaming, as often found within magnetic clouds. Observed in detail, the electron distribution in pitch angle (figure not shown) indicates that the 250 eV electron population in the first period 0830–1000 UT is strongly increased in the parallel direction, especially within 0–60°, but this increase also extends to the antiparallel direction up to 110°. Approximately the opposite is observed during the second active period 1600–1820 UT, i.e., an enhancement in the antiparallel direction extending to pitch angles below 90°. In both cases, the increase is bursty in time in the same manner as the whistler activity. This is consistent with the analysis below of the captured electron distributions.

The electron data comes from the solid state analyzer EESA-low from the Three-Dimensional Plasma experiment (3DP) on WIND [*Lin et al.*, 1995]. The EESA-low instrument observes electrons of energy below 1.2 keV, i.e., of velocity below 20 10^3 km s^{-1}. The lower observational energy is dictated by the spacecraft potential. The data is processed in two formats: the "full" distribution is a cut in a plane containing the IMF, while the "reduced" distributions in the parallel and perpendicular direction ($f_{\|}$ and $f_{\perp}$) result from an integration of this full distribution in the perpendicular and parallel directions, respectively. The data on board is originally expressed in spherical coordinates, transformed into cartesian GSE coordinates, from which the $\mathbf{B}$ direction is attainable, a cut is chosen that includes $\mathbf{B}$, and the data is translated into the solar wind frame by localizing the center of the bulk protons. The electron distribution is not corrected for spacecraft potential. Therefore the density and temperature of the core population are not quantitatively trustworthy, but the effects are negligible at high energy, for example, for the halo population. The phase space distribution has been interpolated from its energy-angle dependence to a regularly spaced grid of two-dimensional velocity space, with velocity ranging from -20–+20 10^3 km s^{-1}.

To cover the active periods, 288 electron distributions were investigated over the joint periods 0730–0926 UT and 0930–1126 UT, 1530–1726 UT and 1728–1924 UT (small data gap in between them). Distributions are sampled over a

spacecraft spin period ($\sim$ 3 s) every 90 s. The electron distributions observed during the active periods are compared to a reference electron distribution representative of the quiet periods.

During the selected quiet period at 0730–0822 UT, a representative electron distribution referred as f_{quiet}, is deduced from 33 very similar distributions. For convenience, f_{quiet} is defined as the maximum value of all the electron distributions for each velocity space bins, rather than the mean. The reduced distributions of the electron distributions that contributed to f_{quiet} (diamonds) are represented altogether above a contour plot of $f_{\text{quiet}}(v_{\|}, v_{\perp})$ (Figure 5). The electron distribution f_{quiet} splits into an isotropic core population, $T_{c_{\|}} \sim T_{c_{\perp}}$, and a halo population showing some tem-

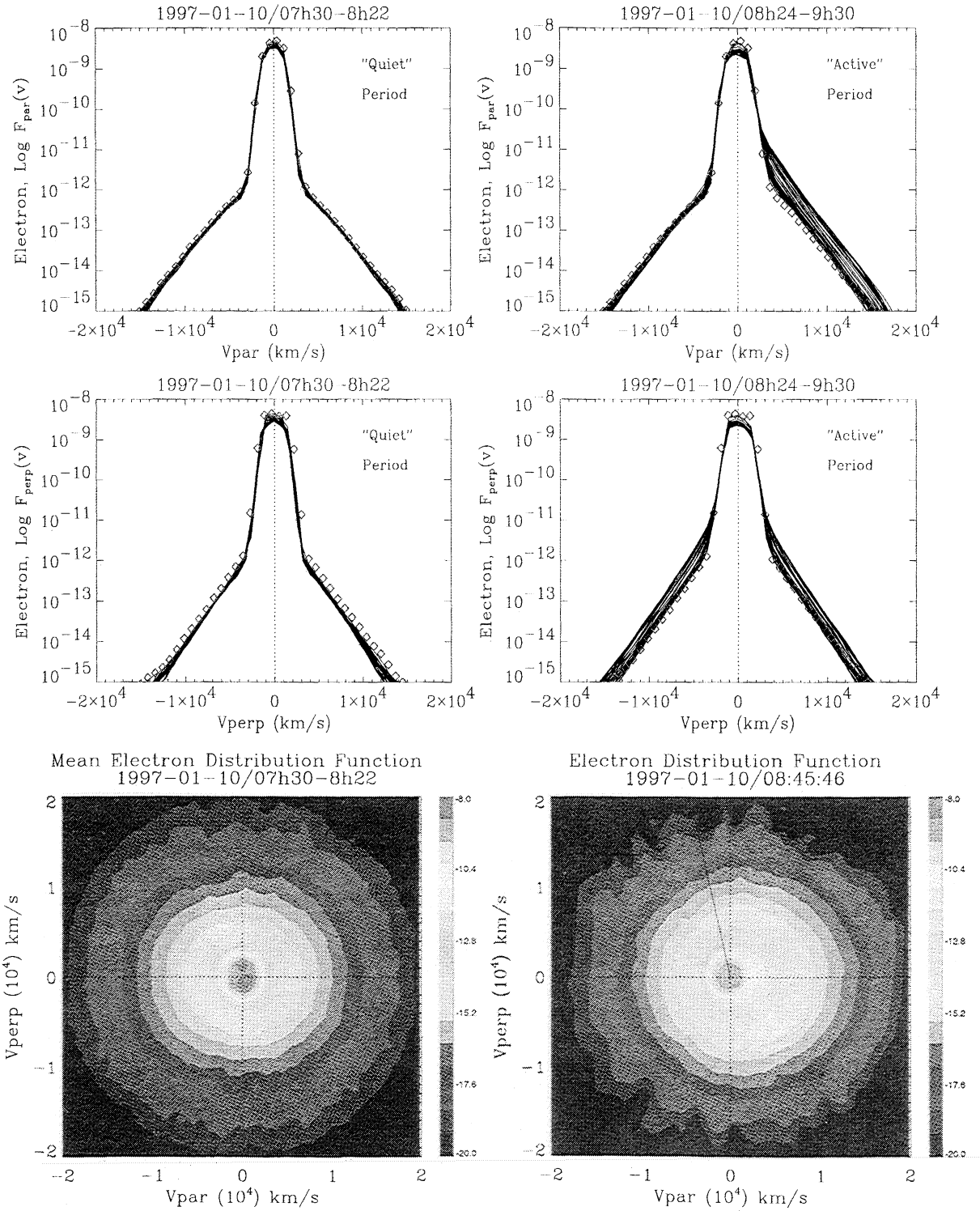

Figure 5. Reduced electron distributions in the parallel and perpendicular direction and two representative two-dimensional distributions. (left) quiet period; (right) first whistler active period 0830–1000 UT.

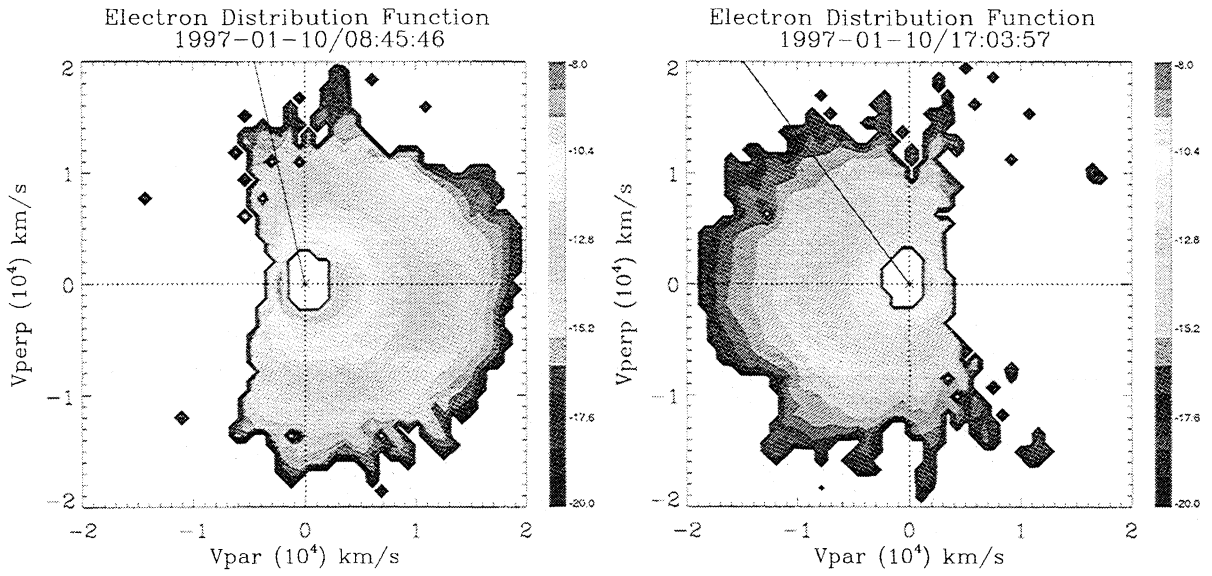

Figure 6. Loss cone representative electron distributions observed at the times of the two whistler active periods inside the January 10, 1997 magnetic cloud. These distributions are obtained by subtracting a mean distribution over the quiet period 0730–0822 UT.

perature anisotropy, $T_{h_\parallel} > T_{h_\perp}$. The break between core and halo occurs around ± 3000 km s^{-1} in the parallel direction and around ± 3250 km s^{-1} in the perpendicular direction. This type of electron distribution relates to the weak "bidirectional heat flux" found in the electron distribution in pitch angle at 250 eV.

All the reduced electron distributions of the first whistler active period are altogether superimposed on the quiet period reduced distribution f_{quiet} (diamonds) above a contour plot of a representative distribution function $f_{w1}(v_\parallel, v_\perp)$ (Figure 5). Relative to f_{quiet}, all electron distributions show an excess of suprathermal electrons. The reduced parallel distribution are strongly asymmetric with a large excess of electrons in the parallel direction, i.e., unidirectional parallel heat flux, and the perpendicular reduced distribution is enlarged (it is symmetric by definition). The break between core and halo occurs around -3250 km s^{-1} and $+2250$ km s^{-1} in the parallel direction (asymmetric) and ± 2750 km s^{-1} in the perpendicular direction. The simplest space velocity geometry dependence that one could infer from the reduced distributions and their gaussian fits is that of an extra electron hot beam population additional to the quiet period distribution.

Subtracting the electron distribution found in the quiet period to the electron distributions during the active period reveals neatly the geometry of the extra suprathermal population: it is a single loss cone distribution. Apparently, this loss cone does not extend to the lowest energies, possibly implying some scattering at low energy. This additional loss cone is shown for a representative active period distribution f_{w1} (Figure 6). For graphical convenience, negative values are "zeroed" to 10^{-20}. Note that the central part of the difference distribution is not meaningful but owing to small fluctuations in the high counts at low energy resulting in large differences. In Figure 6, the direction of the solar wind is shown by a solid line from the origin. The loss of electrons is in the antiparallel direction, antisunward, and the angular (half) width of the loss cone is on average $\alpha_c = 70°$ (varying between 60° and 80°).

To summarize, the excess population (actually denser than the rest of the halo population) found in the first active period appears as a suprathermal loss cone distribution in the antiparallel direction (sunward). During the second active period, the situation is opposite, i.e., the resulting loss cone is in the antiparallel direction and sunward orientated. This time, the break between core and halo occurs around -2500 km s^{-1} and $+2750$ km s^{-1} in the parallel direction and ± 2750 km s^{-1} in the perpendicular direction.

Loss cones are generally attributed to magnetic mirroring: only the particles with direct pitch angle $\alpha > \alpha_c$ (in 0–90°) are reflected back when the particles move toward a region of stronger field in a magnetic bottle geometry. The loss cone (half) angle is given by $\sin {\alpha_c}^2 = B/B_M$, where B_M is the maximum field amplitude in the bottle or mirror field and B is the local field associated with α. In this assumption, the present loss cones are associated with a weak magnetic mirror $B_M \sim 1.13B \sim 16.8$ nT because of their large angles.

7. Correlation Between Whistler Waves, Langmuir Waves, and Electron Loss Cone Distributions

The loss cone distributions are very well correlated in time with the whistler activity (Figure 7). For this, a time series of the magnetic field was calculated from the FFTM spectrogram by summing over a frequency range (69–282 Hz) including the observed frequency bandwidths of both whistler

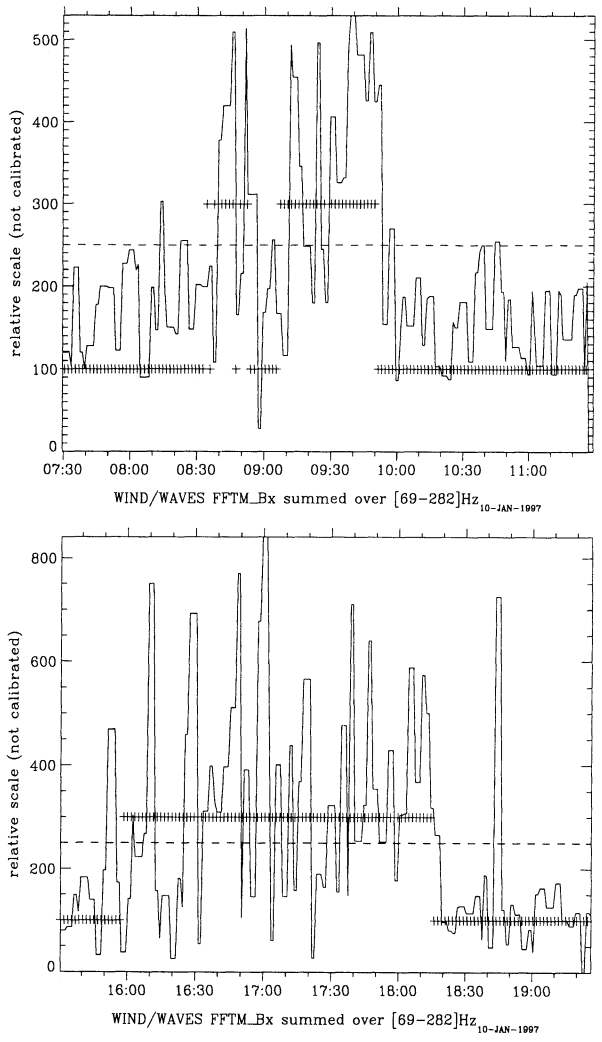

Figure 7. Magnetic time series from FFTM within the whistlers frequency range and electron distribution times during the two whistler active periods on January 10, 1997. The ordinate line at 250 is an indicative threshold of the whistler wave activity relative to the entire day. The times of electron distribution capture are marked with vertical crosses: loss cone at 300, others at 100.

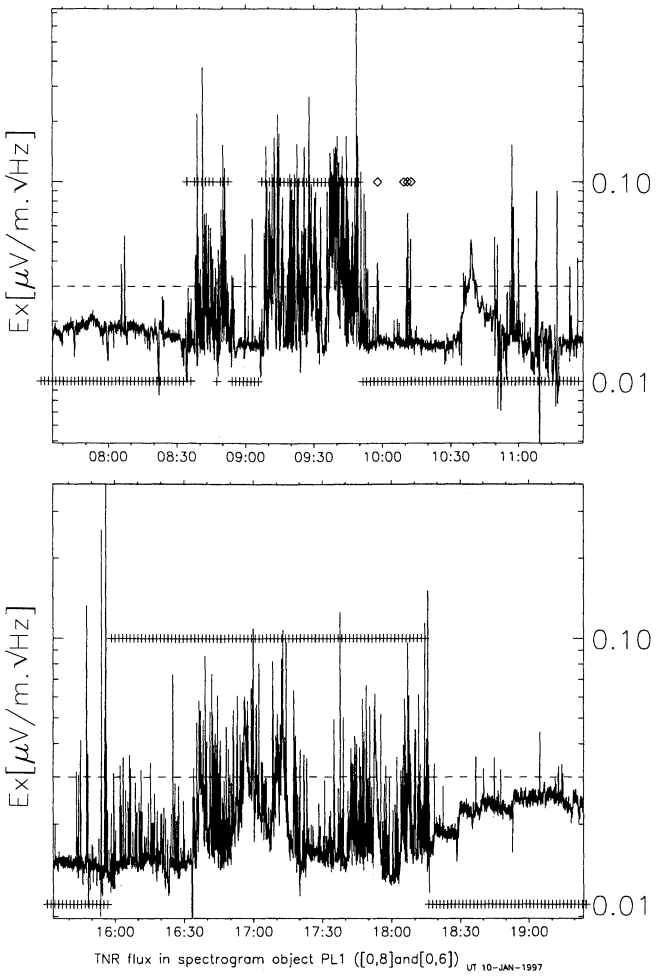

Figure 8. Time series of the electric field intensity within the plasma line from TNR and electron distribution times, during the two whistler active periods on January 10, 1997. The ordinate line at 0.1 is an indicative threshold of the $f_{\mathrm{p_e}}$ wave activity relative to the entire day. The times of electron distribution capture are marked with vertical crosses: loss cone at 0.1, others at 0.01.

periods. The ordinate line at 250 is an indicative threshold of wave activity relative to the entire day, though the amplitudes are not calibrated. The times of electron distribution captures are marked with vertical crosses: at ordinate 300 for the loss cones and at ordinate 100 for the other types of difference distributions (noise remnants or very weak beam-like). Very weak loss cone distributions were not considered loss cone and do not correlate to the whistler activity, which would imply that the density of the loss cone matters.

The loss cone distributions are also very well correlated in time with the Langmuir wave activity (Figure 8). For this, a time series of the electric field intensity was calculated from the TNR spectrogram by integrating the electric field intensity within the plasma line using the spectro-object method to track the changing frequency range of the plasma line [*Moullard*, 2000]. This was done for both whistler periods. The ordinate line at 0.1 μV m^{-1} Hz$^{-\frac{1}{2}}$ is an indicative threshold of wave activity relative to the entire day. The times of electron distribution captures are marked with vertical crosses: at ordinate 0.1 μV m^{-1} Hz$^{-\frac{1}{2}}$ for the loss cones and at ordinate 0.01 μV m^{-1} Hz$^{-\frac{1}{2}}$ for the other types of difference distributions.

8. Toward a Linear Instability Study

The distributions described clearly have the potential to be unstable to wave growth. The observed correlation between wave activity and distribution type (Figures 7 and 8) indicates that the waves are observed within their source region, so that, in the source region, the particle distribution is unstable to, possibly, both whistler and Langmuir waves. This possibility will be explored by using a linear dispersion solver called WHAMP [*Ronnmark*, 1982], which can give the (exact) dispersion relation $\tilde{\omega}(k)$ for a plasma consisting

Table 2. Parameters Obtained From Fitting the Electron Distributions During the Whistler Active and Quiet Periods .

Parameter	Quiet	Active 1	Active 2
n, cm^{-3}	7.1	4.7	6.6
f_{p_e}, kHz	24.0	19.5	23.1
B, nT	15.2	14.8	14
ω_{c_e}, rad s^{-1}	2673.4	2603.1	2462.4
f_{c_e}, Hz	425.5	414.3	391.9
F_0: A_0	8.0 10^{-9}	5.0 10^{-9}	5.0 10^{-9}
F_0 : A_1	0	0	0
F_0 : A_2	780	500	500
F_0 : A_3	820	500	500
F_0: v_t, km s^{-1}	1103.1	707.1	707.1
F_0: $\beta_{\|}$	4.28 10^{-2}	1.23 10^{-2}	1.93 10^{-2}
F_0: $T_\perp/T_{\|}$	1.1	1.0	1.0
F_1: A_0	9.3 10^{-13}	1.29 10^{-11}	1.12 10^{-11}
F_1 : A_1	-13.6	1454	-1415
F_1 : A_2	3713	2490	2432
F_1 : A_3	3447	2683	2559
F_1: n_1/n_0	5.5 10^{-4}	1.28 10^{-2}	1.1 10^{-2}
F_1: v_t, km s^{-1}	5251	3521.4	3439.4
F_1: v_d/v_t	0	0.413	-0.411
F_1: $T_{1,\|}/T_{0,\|}$	22.66	24.8	23.7
F_1: $T_\perp/T_{\|}$	0.86	1.16	1.11
F_2: A_0	3.71 10^{-14}	6.51 10^{-13}	4.65 10^{-13}
F_2 : A_1	0	-13.6	-3000
F_2 : A_2	5198	3713	3713
F_2 : A_3	4826	4136	4309
F_2: $T_\perp/T_{\|}$	1.1	1.24	1.35
F_3: A_0		6.51 10^{-13}	1.55 10^{-14}
F_3 : A_1		3100	8500
F_3 : A_2		3713	1485
F_3 : A_3		3713	1485

F_0, core fit; F_1, F_2, F_3, halo fits.

of a sum of bi-Maxwellian distributions. This will be the subject of a second paper.

In view of the linear instability study, we report here the results of a fitting procedure to the electron distributions for periods with and without whistler activity. The fitting procedure used three to four Maxwellians to fit the reduced parallel and perpendicular distribution functions. The justification for using this type of fit, despite having an extra population that clearly does not have a bi-Maxwellian form, will be given in the next paper. The results of the fitting procedure are shown in Table 2. The electron particle distribution function is assumed of the form

$$f(v_{\|}, v_\perp) = \sum_i A_{0_i} \exp -\frac{1}{2}\left[\left(\frac{v_{\|} - A_{1_i}}{A_{2_i}}\right)^2 + \left(\frac{v_\perp}{A_{3_i}}\right)^2\right],$$

where the A parameters are adjusted to fit the observations. In Table 2 some relevant relative values are also extracted. Note that since the core of the electron distribution is not well-resolved, we actually use the density from the 3DP ion instrument for ω_{p_i}, and from the electron data we extract the relative densities of the various components. This will not be extremely accurate, but we only need to approximately characterize the distributions, so that we can define model distributions for the instability study.

9. Discussion

To summarize, there is within this magnetic cloud a strong observational case of wave particle activity with time and intensity correlated Langmuir waves, whistler waves (propagating along the magnetic field) and electron loss cone distributions. At the same time, type II bands are observed at near the local $2f_{p_e}$ and side bands around f_{p_e}. So it is tempting to speculate that some type II emission mechanisms are taking place: parametric decay involving Langmuir waves ($L + L' \rightarrow T(2f_{p_e})$) and perhaps whistler waves could well occur. Additionally, there is no sign of local type II emission activity in the sheath or in the foreshock of the interplanetary magnetic cloud. Perhaps, type II emission is proceeding inside the magnetic cloud, instead of taking place in the shock region as usually thought.

The time correlation between the single loss cones occurrence and the whistler and Langmuir waves activity is excellent. During the second active period, where whistler waveforms are observed, the single loss cone present a loss in the antiparallel direction, the loss cone direct pitch angle is $\alpha_c = 70°$.

Are the observed loss cone distributions unstable to both whistler and Langmuir waves and how? A preliminary study (not presented here) found the electron distribution linearly unstable to both waves with properties closely matching the observed. The electron distribution was simply modeled as a beam, i.e., no loss cone features were accounted for, using observed properties based on the multicomponent Maxwellian fits on the reduced distributions (shown here). The instability study also puts a constraint on the direction of the whistler wave vector: parallel to $\mathbf{B}_0$ when the loss of electrons is in the antiparallel direction (and vice versa). This is quite incompatible with the classical electron cyclotron mechanism that predicts a wave vector aligned with the loss direction. The results of this work are to be delivered in a following article.

The issue of the source of the suprathermal electrons is extremely interesting. The single loss cone features in the distribution match an electron beam mirrored within the magnetic cloud or erosion of the pitch angle distribution by interaction with the whistler waves. A number of possibilities for the origin of such a beam can be suggested: remote connection to an interplanetary shock associated with the magnetic cloud, a burst from coronal source (unlikely), connection to a reconnection site between the magnetic cloud and its surrounding sheath or ambient solar wind structures. A quick investigation of the cloud geometry indicates that the active sites could be located on the same flux surface in the outer part of the magnetic cloud.

Appendix A: Whistler Wave Dispersion Relation in the Observed Frame

The whister wave dispersion relation is traditionally expressed in the refractive index form $n^2(\omega)$

$$\frac{k^2c^2}{\omega^2} = \frac{\omega_{p_e}^2}{\omega(\omega_{c_e}\cos\theta_{kB} - \omega)}.$$

Choosing

$$\tilde{\omega} = \omega/\omega_{c_e}\cos\theta_{kB} \text{ and } \tilde{k} = kc/\omega_{p_e}$$

simplifies nicely the dispersion relation to

$$\tilde{k}^2 = \frac{\tilde{\omega}}{1-\tilde{\omega}}$$

then easily inversed

$$\tilde{\omega} = \frac{\tilde{k}^2}{1+\tilde{k}^2}$$

substituting back gives the dispersion in the form $\omega(k)$

$$\omega = \frac{\omega_{c_e}\cos\theta_{kB}k^2}{k^2 + \frac{\omega_{p_e}^2}{c^2}}.$$

The system formed by the dispersion and doppler shift relations

$$\begin{cases} \omega' = \omega + \mathbf{k}\cdot\mathbf{V} \\ \omega = \frac{\omega_{c_e}\cos\theta_{kB}k^2}{k^2+\frac{\omega_{p_e}^2}{c^2}} \end{cases}$$

with knowns $\omega_{p_e}, \omega_{c_e}, \theta_{kB}, V, \theta_{kV}, \omega'$, and unknowns f, ω, is solved for k giving the cubic equation

$$\begin{aligned} 0 \quad &= \pm k^3(V\cos\theta_{kV}) + k^2(\omega_{c_e}\cos\theta_{kB} - \omega') \\ &\pm k(\tfrac{\omega_{p_e}^2}{c^2}V\cos\theta_{kV}) - \omega'\tfrac{\omega_{p_e}^2}{c^2}. \end{aligned}$$

This equation is degenerated in two cases corresponding to a positive or negative doppler shift $\mathbf{k}\cdot\mathbf{V} = \pm kV\cos\theta_{kV}$. This equation represents the whistler wave dispersion relation in the observed frame.

Acknowledgments. We thank the WIND WAVES team, in particular Mike Kaiser (Principal Investigator of WAVES, GSFC), Jean-Louis Bougeret (co-PI, Meudon) and Paul Kellogg (PI of TDS, Minnesota) for their permission to use the WIND WAVES data, as well as K. Goetz, J. Kappler, C. Meetre, and S. Monson (Minnesota) for the TDS instrument and the Windlib database software. We are grateful to the WIND 3DP team (PI, Bob Lin, Berkeley) for the electron distribution data. And we thank the WIND MFI (PI, R. Lepping, GSFC) and SWE (PI, Keith Ogilvie) teams for essential solar wind parameter data.

The Editor, Hiroshi Matsumoto, thanks H. Kojima and another referee for their assistance in evaluating this paper.

References

Bale, S. D., M. J. Reiner, J. L. Bougeret, M. L. Kaiser, S. Krucker, D. E. Larson, and R. P. Lin, The source region of an interplanetary type II radio burst, *Geophys. Res. Lett.*, *26*(11), 1573–1576, 1999.

Bougeret, J. L., et al., WAVES: the radio and plasma wave investigation on the WIND spacecraft, *Space Sci. Rev.*, *71*(1-4), 231–263, 1995.

Buhler, P., A. Johnstone, L. Desorgher, A. Zehnder, E. Daly, and L. Adams, The outer radiation belt during the 10 January, 1997 CME event, *Geophys. Res. Lett.*, *25*(15), 2983–2986, 1998.

Burlaga, L. F., Magnetic clouds, *in Physics of the inner heliosphere II*, edited by R. Schwenn and E. Marsch, Springer-Verlag, Berlin Heidelberg New York, 1991.

Burlaga, L., et al., A magnetic cloud containing prominence material: January 1997, *J. Geophys. Res.*, *103*(A1), 277–285, 1998.

Chian, A. C. L., and J. R. Abalde, Nonlinear coupling of Langmuir waves with whistler waves in the solar wind, *Sol. Phys.*, *184*(2), 403–419, 1999.

Fox, N. J., M. Peredo, and B. J. Thompson, Cradle to grave tracking of the January 6-11, 1997 Sun-Earth connection event, *Geophys. Res. Lett.*, *25*(14), 2461–2464, 1998.

Kellogg, P. J., K. Goetz, N. Lin, S. J. Monson, A. Balogh, R. J. Forsyth, and R. G. Stone, Low-frequency magnetic signals associated with Langmuir waves, *Geophys. Res. Lett.*, *19*(12), 1299–1302, 1992.

Kellogg, P. J., K. Goetz, S. J. Monson, and S. D. Bale, A search for Langmuir solitons in the Earth's foreshock, *J. Geophys. Res.*, *104*(A4), 6751–6757, 1999.

Kennel, C. F., F. L. Scarf, F. V. Coroniti, R. W. Fredricks, D. A. Gurnett, and E. J. Smith, Correlated whistler and electron plasma oscillation bursts detected on ISEE 3, *Geophys. Res. Lett.*, *7*(2), 129–132, 1980.

Kurth, W. S., T. Murata, G. Lu, D. A. Gurnett, and H. Matsumoto, Auroral kilometric radiation and the auroral electrojet index for the January 1997 magnetic cloud event, *Geophys. Res. Lett.*, *25*(15), 3027–3030, 1998.

Larson, D. E., R. P. Lin, and J. Steinberg, Extremely cold electrons in the January 1997 magnetic cloud, *Geophys. Res. Lett.*, *27*(2), 157–160, 2000.

Lengyelfrey, D., W. M. Farrell, R. G. Stone, A. Balogh, and R. Forsyth, An analysis of whistler waves at interplanetary shocks, *J. Geophys. Res.*, *99*(A7), 13325–13334, 1994.

Lin, N. G., P. J. Kellogg, R. J. Macdowall, A. Balogh, R. J. Forsyth, J. L. Phillips, A. Buttighoffer, and M. Pick, Observations of plasma waves in magnetic holes, *Geophys. Res. Lett.*, *22*(23), 3417–3420, 1995.

Mangeney, A., et al., Wind observations of coherent electrostatic waves in the solar wind, *Ann. Geophys.*, *17*(3), 307–320, 1999.

Moullard, O., Observations of plasma waves in the solar wind, Ph.D. thesis, Univ. of London, London, United Kingdom, 2000.

Moullard, O., D. Burgess, and S. D. Bale, Whistler waves observed during an in situ solar type III radio burst, *Astron. Astrophys.*, *335*(2), 703–708, 1998.

Mulligan, T., C. T. Russell, and J. G. Luhmann, Solar cycle evolution of the structure of magnetic clouds in the inner heliosphere, *Geophys. Res. Lett.*, *25*(15), 2959–2962, 1998.

Phillips, J. L., W. C. Feldman, J. T. Gosling, C. M. Hammond, and R. J. Forsyth, Suprathermal electron loss cone distributions in the solar wind: Ulysses observations, in Solar Wind Eight, edited by D. Winterhalter et al., *AIP Conf. Proc.* , 382, 293–296, 1996.

Pilipp, W. G., H. Miggenrieder, K. H. Muhlhauser, H. Rosenbauer, R. Schwenn, and F. M. Neubauer, Variations of electron distribution functions in the solar wind, *J. Geophys. Res.*, *92*(A2), 1103–1118, 1987.

Reiner, M. J., M. L. Kaiser, J. Fainberg, J. L. Bougeret, and R. G. Stone, On the origin of radio emissions associated with the January 6-11, 1997, CME, *Geophys. Res. Lett.*, *25*(14), 2493–2496, 1998a.

Reiner, M. J., M. L. Kaiser, J. Fainberg, and R. G. Stone, A new method for studying remote type II radio emissions from coro-

nal mass ejection-driven shocks, *J. Geophys. Res.*, *103*(A12), 29,651–29,664, 1998b.

Ronnmark, K., WHAMP: Waves in Homogeneous Anisotropic Multicomponent Plasmas, *KGI report*, *179*, Kiruna,1982.

Thejappa, G., and R. J. Macdowall, Evidence for strong and weak turbulence processes in the source region of a local type III radio burst, *Astrophys. J.*, *498*(1 Pt1), 465–478, 1998.

Thejappa, G., D. G. Wentzel, R. J. Macdowall, and R. G. Stone, Unusual wave phenomena near interplanetary shocks at high latitudes, *Geophys. Res. Lett.*, *22*(23), 3421–3424, 1995a.

Thejappa, G., D. G. Wentzel, and R. G. Stone, Low-frequency waves associated with Langmuir waves in solar wind, *J. Geophys. Res.*, *100*(A3), 3417–3426, 1995b.

Webb, D. F., E. W. Cliver, N. Gopalswamy, H. S. Hudson, and O. C. Stcyr, The solar origin of the January 1997 coronal mass ejection, magnetic cloud and geomagnetic storm, *Geophys. Res. Lett.*, *25*(14), 2469–2472, 1998.

S. D. Bale and D. E. Larson, Space Sciences Laboratory, University of California, Berkeley, CA 94720-7450. (davin@ssl.berkeley.edu; bale@apollo.ssl.berkeley.edu)

D. Burgess, Astronomy Unit, Queen Mary and Westfield, Mile End Road, London E14NS, UK. (d.burgess@qmw.ac.uk)

A. Mangeney and C. Salem, DESPA, Observatoire de Paris-Meudon, 92195 Meudon Cedex, France. (andre.mangeney@obspm.fr; chadi.salem@obspm.fr)

O. Moullard, Space Science Department, ESTEC, ESA, Postbus 299, 2200 AG Noordwijk, Netherlands. (om@so.estec.esa.nl)

(Received April 21, 2000; revised August 28, 2000;
accepted October 11, 2000.)